Performance of an Aerospace Plane Propulsion Nozzle

Yoon-Yeong Bae* and George Emanuel†
University of Oklahoma, Norman, Oklahoma 73069

A novel inviscid and viscous analysis is provided for a nozzle that is used with a scramjet for thrust generation. The analysis is based on the theory of a two-dimensional minimum length nozzle with a curved inlet surface, where the flow is sonic or supersonic. Inlet conditions are prescribed and the gas is assumed to be perfect. Viscous and inviscid nondimensional parametric results are provided for the thrust, lift, heat transfer, pitching moment, and a variety of boundary-layer thicknesses. In addition to global results, wall distributions of thrust, heat transfer, etc., are provided. The analysis demonstrates that the nozzle produces a lift force whose magnitude may exceed the thrust and a significant pitching moment. The thrust is sensitive to the inlet Mach number; it rapidly decreases as this Mach number increases. There is little loss in the thrust as the nozzle's downstream wall is truncated while the corresponding decrease in lift and the pitching moment is moderate.

Nomenclature

A = cross-sectional area
A,A',B,B',C' = special wall points
a,b,c = wall sections of the nozzle
C = Chapman-Rubesin parameter, $=\rho\mu/(\rho_e\mu_e)$
C_F,C_L,C_M,C_Q = nondimensional thrust, lift, pitching moment, and heat transfer coefficients
C_t,C_v = parameters (see Ref. 8)
C_μ = viscosity constant, $=\mu/T$
C_+,C_- = left and right running characteristics, respectively
c_f = skin-friction coefficient, $=2\tau_w/(\rho_e u_e^2)$
$\hat{e}_x,\hat{e}_y,\hat{e}_z$ = Cartesian basis
F_r,M_r,Q_r = reference values for the thrust and lift, pitching moment, and heat transfer
F_p,F_τ = forces due to pressure and skin friction
f''_w = velocity gradient at the wall
G'_w = enthalpy gradient at the wall
g_w = stagnation temperature ratio, $=T_w/T_{oe}$
H_i = see Table 1
h = enthalpy
K = constant defined by Eq. (17)
l = length defined by Eq. (5)
M = Mach number
M_p,M_τ = pitching moments due to pressure and skin friction
$\dot{m}$ = mass flow rate
Pr = Prandtl number
p = pressure
Q = integrated wall heat transfer
q_w = local wall heat transfer
R = radius
Re_o = Reynolds number defined by Eq. (10)
R_g = specific gas constant
s = arc length along the wall
T = temperature
u = velocity component parallel to the wall
V = flow speed
$\bar{x}$ = nondimensional length defined by Eq. (25)
x,y,z = coordinates defined in Fig. 1
β = pressure gradient parameter
γ = specific heat ratio
$\delta,\delta_t,\delta^*,\theta,\phi$ = velocity, thermal, displacement, momentum, and stagnation enthalpy thicknesses
θ = angle between velocity and the x coordinate
θ^* = initial expansion angle for the upper wall of the nozzle
η = boundary-layer similarity variable
η_{et},η_{ev} = η value at the thermal and velocity boundary-layer edges
ξ = transformed coordinate along the wall
μ = viscosity
ρ = density
τ_w = wall shear stress
ω = $\theta^* - \nu_f + \nu$
Υ = $[(\rho_e u_e \bar{x}\tilde{z}_i)/2\mu_e]^{1/2}/(\bar{x}\tilde{z}_i)$

Subscripts and Superscripts

e = edge of the boundary layer
f = nozzle exit plane
i = initial data line
inv = inviscid part of a performance parameter
o = stagnation condition
p = pressure contribution
r = reference value
tr = truncation
vis = viscous part of a performance parameter
w = wall condition
τ = shear stress contribution
$(\tilde{\ })$ = dimensional spatial variable
$(\hat{\ })$ = normalized quantity
$(\ )'$ = upper nozzle wall
$(\ )'$ = derivative with respect to the similarity variable
$(\ )_m,(\ )_M$ = optimum conditions for θ^*

Mach Number Functions

$F = MX^{-(3\gamma-1)/2(\gamma-1)}$

$I(M) = 2(M^2-1) + [(\gamma+1)/2]M^4(M^2-1)^{-1/2}\omega$

$J(M,M_i) = \ell n\left[\frac{M_i}{M}\left(\frac{X}{X_i}\right)^{1/2}\right] + \frac{\gamma+1}{2(\gamma-1)}\left(\frac{1}{X_i}-\frac{1}{X}\right)$

$S = \frac{[(\gamma-1)/2]M^2}{1+[(\gamma-1)/2]M^2}$

$X = 1+[(\gamma-1)/2]M^2$

Received May 20, 1989; presented as Paper 89-1878 at the AIAA 20th Fluid and Plasma Dynamics Conference, Buffalo, NY, June 12–14, 1989; revision received Feb. 26, 1990.

*Graduate Student, Department of Aerospace and Mechanical Engineering. Member AIAA.
†Professor, Department of Aerospace and Mechanical Engineering. Associate Fellow AIAA.

$$\alpha = (M_i/M)(X/X_i)^{(\gamma+1)/2(\gamma-1)}$$

$$\nu = \left(\frac{\gamma+1}{\gamma-1}\right)^{1/2} \tan^{-1}\left[\left(\frac{\gamma-1}{\gamma+1}\right)^{1/2}(M^2-1)^{1/2}\right] - \tan^{-1}(M^2-1)^{1/2}$$

$$\mu = \sin^{-1}(1/M)$$

I. Introduction

A BLENDED forebody configuration for the aerospace plane suggests the use of the upper half of a minimum length nozzle (MLN) for the afterbody. The shape of the afterbody can be based on the theory of a two-dimensional MLN with a circular inlet surface. Figure 1 shows a schematic of the nozzle, where flow at the inlet is a supersonic source flow and the exit flow is uniform. A two-dimensional nozzle is appropriate for the compressive flowfield produced by the forebody and takes advantage of the lift that is generated by the pressure on the nozzle's upper wall. Of the various MLN configurations, only the two-dimensional one with a curved inlet line, or surface, possesses a complete inviscid analytical solution.[1] Further discussion of MLNs, including additional references, is contained in Refs. 2 and 3.

Our objective is to provide comprehensive nondimensional parametric results that establish trends and reference criteria against which alternate approaches can be compared. Global results are emphasized that provide thrust, lift, heat transfer, pitching moment, and boundary-layer thicknesses. In addition, selected wall distributions of various parameters are given. Of course, both types of results are essential for design studies.

Since this is an initial treatment of a scramjet thrust nozzle, we have kept the analysis as simple as possible with emphasis on an analytical formulation. An important second objective is, therefore, to establish a general viscous methodology that later can be used for other nozzle configurations and flow conditions.

In line with these goals, a number of simplifying assumptions are involved. The two most important are the use of a thermally and calorically perfect gas and a two-dimensional flow. For the viscous computation, we utilize locally similar, laminar boundary-layer theory with the Prandtl number and Chapman-Rubesin parameter equal to unity. The laminar assumption is not necessarily unrealistic, since a characteristic nozzle Reynolds number turns out to be rather small and the boundary layers experience a large favorable pressure gradient inside the nozzle.

A number of topics are discussed in Ref. 4 that are omitted here. These include justification of local similarity and the unity values for the Prandtl number and Chapman-Rubesin parameter. This reference also discusses the momentum theorem, which is used to verify the inviscid formulation, Reynolds analogy, the transfer of the pitching moment to a different coordinate system, how singular integrals are analytically and numerically treated, and the various numerical methods utilized.

II. Inviscid Formulation

Any MLN with a sonic line inlet has a cusped wall[1] at the throat (point A' in Fig. 1). When $M_i > 1$, neither wall has a cusp, and Fig. 1 is drawn for this case. Of course, a cusp in the wall results in severe heat transfer and may lead to boundary-layer separation.[3] The no-cusp situation is therefore desirable. Our inviscid analysis of the half nozzle is kept brief, since it parallels Ref. 1, which is for a conventional two-dimensional MLN with a curved sonic line. Some details, however, are essential for clarity and for the subsequent viscous analysis because we have half of a nozzle whose inlet is not necessarily sonic.

In accord with MLN theory, the flow in region $AA'B'B$ is a source flow whose (apparent) center is the origin of the coordinate system. Although this is a nonsimple wave region, we have the usual isentropic area relation:

$$\frac{A}{A^*} = \frac{1}{M}\left(\frac{2X}{\gamma+1}\right)^{(\gamma+1)/2(\gamma-1)} \tag{1}$$

The mass flow rate, per unit depth, is given by

$$\dot{m} = (\rho A V)_i = \frac{M_i p_o \tilde{R}_i \theta^*}{X_i^{(\gamma+1)/2(\gamma-1)}}\left(\frac{\gamma}{R_g T_o}\right)^{1/2} \tag{2}$$

where the inlet angle θ^* is determined later. A tilde indicates a dimensional length, whereas lengths without a tilde are normalized with the inlet height $\tilde{z}_i$. Since $A = \tilde{R}\theta^*$, we obtain a functional relation that is used in the subsequent analysis by combining Eqs. (1) and (2):

$$\tilde{R}/\tilde{R}_i = A/A_i = (M_i/M)(X/X_i)^{(\gamma+1)/2(\gamma-1)} = \alpha(M;M_i) \tag{3}$$

Other useful relations in the source flow region are

$$\theta = \nu(M_f) + \nu(M) = \nu_f + \nu, \qquad C_+ \tag{4a}$$

$$\theta = \nu(M_f) - \nu(M) = \nu_f - \nu, \qquad C_- \tag{4b}$$

where θ is an angle between the velocity and the lower wall, ν is the Prandtl-Meyer function, and C_+ and C_- represent left- and right-running characteristics, respectively.

Region $BB'C'$ in Fig. 1 is a simple wave region. The downstream border BC' is a straight Mach line at a Mach angle μ_f and with a Mach number M_f. To determine the wall contour $B'C'$, we equate the mass flow rates through PP'' and PP', where P'' is on the linear extension of $A'B'$ and P' is on the contour $B'C'$, to obtain

$$\tilde{l}/\tilde{R} = (\theta^* - \theta)/\sin\mu = M(\theta^* - \theta) \tag{5}$$

Then, the coordinates of the contour $B'C'$ are given by

$$x/R = \cos\theta + (l/R)\cos(\theta+\mu) \tag{6a}$$

$$z/R = \sin\theta + (l/R)\sin(\theta+\mu) \tag{6b}$$

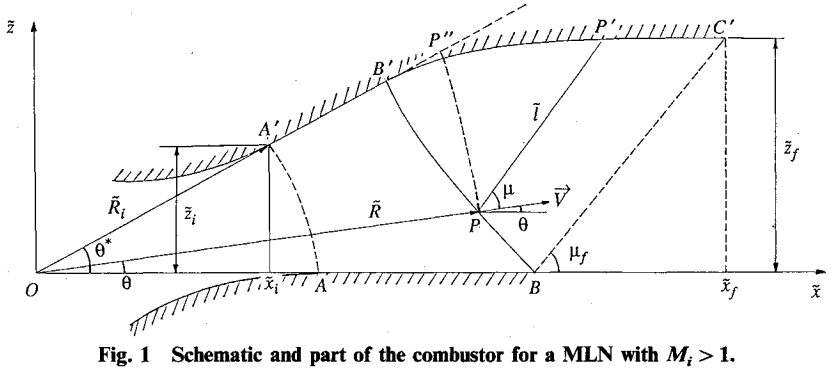

Fig. 1 Schematic and part of the combustor for a MLN with $M_i > 1$.

where R, θ, l/R, and μ are functions of the parameter M, which is the constant Mach number along the PP' Mach line.

The nozzle length is given by

$$x_f - x_i = \alpha_f \theta^* \csc\theta^* \cot\mu_f + \alpha_f \csc\theta^* - \cot\theta^* \tag{7}$$

The initial expansion angle θ^* is θ^*_M, which minimizes the nozzle length.[1] This θ^*_M result holds when point B' differs from A'. When these points coincide, at low M_f, θ^* equals θ^*_m, which is given by

$$\theta^*_m = \nu_f - \nu_i \tag{8}$$

The coordinates of the points along the curved wall contour $B'C'$ are determined by setting θ^* equal to θ^*_M or θ^*_m, whichever is smaller. Substitution of Eqs. (3) and (5) into Eqs. (6) yields

$$x = \alpha \csc\theta^*\{\cos(\nu_f - \nu) + \omega[(M^2-1)^{1/2}\cos(\nu_f - \nu) - \sin(\nu_f - \nu)]\} \tag{9a}$$

$$z = \alpha \csc\theta^*\{\sin(\nu_f - \nu) + \omega[(M^2-1)^{1/2}\sin(\nu_f - \nu) + \cos(\nu_f - \nu)]\} \tag{9b}$$

where ω, along with other symbols, is defined in the Nomenclature. With all lengths normalized by $\tilde{z}_i$, the flowfield in region $AA'C'B$ is fully determined by specifying γ, M_i, and M_f. To determine the radius $\tilde{R}_i$, it is also necessary to specify $\dot{m}(R_gT_o)^{1/2}/p_0$.

Figure 2 shows θ^* for different M_i values when $\gamma = 1.4$. Along the vertically oriented curves, $B' = A'$, there is no planar wall section in the upper wall, and $\theta^* = \theta^*_m$. As M_f increases, we move to the more horizontal curve, where there is a planar section and $\theta^* = \theta^*_M$.

III. Viscous Formulation

We designate the lower wall with an a subscript; b and c, respectively, denote the straight and curved sections of the upper wall. For each section, boundary-layer parameters such as β, τ_w, and q_w are obtained. The analysis assumes a boundary layer that may be already developed at the inlet of the nozzle. For the boundary layer, β and g_w define local flow conditions, where β is determined by the inviscid flow along the wall. As a result of the perfect gas assumption and the Chapman-Rubesin parameter equal to unity, we have $\mu = C_\mu T$. For later convenience, we replace C_μ in terms of a Reynolds number Re_o that is based on stagnation conditions, the maximum flow speed, and the nozzle inlet height:

$$Re_o = \frac{\rho_o(2h_o)^{1/2}\tilde{z}_i}{\mu_o} = \left(\frac{2\gamma}{(\gamma-1)R_g}\right)^{1/2}\frac{p_o\tilde{z}_i}{C_\mu T_o^{3/2}} \tag{10}$$

The formula for β in the source flow region is different from that in the simple wave region. Separate formulas are, therefore, derived for β for the three wall sections. We first evaluate a general equation[5] for β, defined as

$$\beta = \frac{2\xi}{\mathrm{d}\xi}\frac{\mathrm{d}M}{M} \tag{11}$$

where

$$\xi = \xi_i + \int_0^s (\rho\mu u)_e \,\mathrm{d}s \tag{12}$$

and ξ_i is an arbitrary constant that represents the boundary layer's history upstream of point A. Although the Mach number is evaluated at the edge of the boundary layer, we use M instead of M_e for notational simplicity and the transformed lengths ξ and s have been normalized with $\tilde{z}_i$. From relations evaluated at the edge of the boundary layer[5]

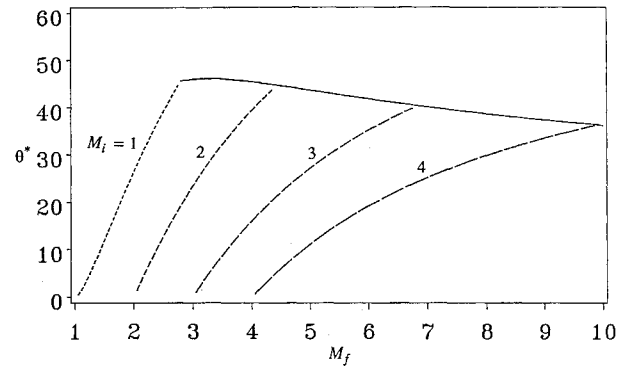

Fig. 2 Initial expansion angle θ^* vs exit Mach number M_f for the inlet Mach number $M_i = 1, 2, 3,$ and 4. Each case is represented by a broken line that continues as a solid line.

$$u_e = (\gamma R_g T_o)^{1/2} M X^{-1/2} \tag{13a}$$

$$\rho_e = (p_o/R_gT_o)X^{-1/(\gamma-1)} \tag{13b}$$

$$\mu_e = C_\mu T_o X^{-1} \tag{13c}$$

the integrand $(\rho\mu u)_e$ becomes

$$(\rho\mu u)_e = \left(\frac{2\gamma^2}{\gamma-1}\right)^{1/2}\frac{p_o^2\tilde{z}_i F}{Re_o R_g T_o} \tag{14}$$

A. Wall Section *a*

Along wall a, the nondimensional wall length is given by $s = x - \csc\theta^*$, where x is obtained from Eq. (3) in terms of the local Mach number by replacing R with x, and s is measured from point A. By differentiating Eq. (3) with respect to M and noticing that $\mathrm{d}R = \mathrm{d}x = \mathrm{d}s$, we have

$$\mathrm{d}s = \frac{\alpha \csc\theta^*(M^2-1)}{X}\frac{\mathrm{d}M}{M} \tag{15}$$

Substitution of Eqs. (14) and (15) into Eq. (12) yields

$$\xi = \xi_i + K\int_{M_i}^{M}\frac{M^2-1}{X^2}\frac{\mathrm{d}M}{M} \tag{16}$$

where the constant K is

$$K = \left(\frac{2\gamma^2}{\gamma-1}\right)^{1/2}\frac{p_o^2\tilde{z}_i \csc\theta^* M_i}{Re_o R_g T_o X_i^{(\gamma+1)/2(\gamma-1)}} \tag{17}$$

From Eq. (11), with

$$\frac{\mathrm{d}\xi}{\mathrm{d}M} = \frac{K(M^2-1)}{MX^2} \tag{18}$$

we obtain β in terms of the parameter M:

$$\beta = \frac{2X^2}{K(M^2-1)}\left(\xi_i + K\int_{M_i}^{M}\frac{M^2-1}{X^2}\frac{\mathrm{d}M}{M}\right)$$

The integral on the right side can be evaluated to yield

$$\beta = \frac{2X^2(\xi_i + KJ)}{K(M^2-1)} \tag{19}$$

where

$$J(M,M_i) = \int_{M_i}^{M}\frac{M^2-1}{X^2}\frac{\mathrm{d}M}{M}$$

$$= \ell n\left[\frac{M_i}{M}\left(\frac{X}{X_i}\right)^{1/2}\right] + \frac{\gamma+1}{2(\gamma-1)}\left(\frac{1}{X_i} - \frac{1}{X}\right)$$

This pressure gradient parameter relation holds for a planar wall with an imposed source flow Mach number distribution, $M = M(s)$. Observe that when $M = M_i$, or $s = 0$, β is proportional to ξ_i. Thus, ξ_i establishes the value of β at the nozzle inlet. As is evident from the $M^2 - 1$ factor in Eq. (19), β is infinite when $M = 1$ with $M_i = 1$ and $\xi_i \neq 0$. However, if $M = M_i = 1$ and $\xi_i = 0$, β is indeterminant. In this circumstance, L'Hospital's rule yields $\beta = 0$.[4]

B. Wall Section *b*

Since both walls *a* and *b* are adjacent to a source flow region, the formulas for wall *a* can be employed with slight modifications. The transformed length ξ_i is replaced with ξ_i', which may be different from ξ_i. With this change, we have

$$\xi' = \xi_i' + KJ, \quad \beta = \frac{2X^2(\xi_i' + KJ)}{K(M^2-1)}, \quad z = x\tan\theta^*_M \tag{20a,b,c}$$

In contrast to the lower wall, the upper wall has a cusp when $M_i = 1$. In this circumstance, we set $\xi_i' = 0$, with the result that $\beta = 0$ at point A'. The length ds is obtained from Eq. (15).

C. Wall Section *c*

The arc length along wall *c* is $ds = [(dx)^2 + (dz)^2]^{1/2}$. By differentiating Eqs. (9) with respect to M, we obtain

$$\frac{dx}{dM} = \frac{\alpha \csc\theta^* I \cos\theta}{MX} \tag{21a}$$

$$\frac{dz}{dM} = \frac{\alpha \csc\theta^* I \sin\theta}{MX} \tag{21b}$$

where $dv = (M^2-1)^{1/2}\,dM/(MX)$ is used. Thus, from Eqs. (21) we obtain

$$ds = \frac{\alpha \csc\theta^* I}{MX}\,dM \tag{22}$$

The transformed length ξ' is given by Eq. (12), which becomes, with Eq. (14),

$$\xi' = \xi_i' + \xi'_{A'B'} + K\int_{M_{B'}}^{M} \frac{I\,dM}{MX^2} \tag{23}$$

where Eq. (22) replaces ds, and $\xi'_{A'B'}$ is given by

$$\xi'_{A'B'} = KJ(M_{B'}, M_i)$$

By differentiating Eq. (23) with respect to M and substituting it into Eq. (11), we obtain $\beta = 2X^2\xi'/(KI)$.

D. Discussion of β

In Fig. 3, the distribution of β along walls *a*, *b*, and *c* is shown for three ξ_i values, with $\xi_i' = \xi_i$. Note that the value of β at the end of wall *b* is larger than its value at the start of wall *c*. This discontinuity stems from the discontinuity in dM/ds, which is in accord with characteristic theory. The dM/ds discontinuity is evident by comparing Eqs. (15) and (22) with $\omega = 0$, which occurs at the junction point, i.e.,

$$\frac{dM}{ds} = \frac{MX}{\alpha \csc\theta^*(M^2-1)}, \quad \text{wall } b$$

$$\frac{dM}{ds} = \frac{MX}{2\alpha \csc\theta^*(M^2-1)}, \quad \text{wall } c$$

Since ξ' is continuous, the 1/2 factor in the latter equation results in a similar discontinuity in β. It should be noted that the local similarity assumption is not appropriate in a small region downstream of this point. Nonsimilar calculations,[6] however, show that the skin friction rapidly relaxes downstream of a discontinuity in β to its value provided by the locally similar solution.

An interesting observation is that when $\xi_i\,(=\xi_i') = 0.05$, which is about 250% of the change in ξ for wall *a*, β does not increase monotonically. Rather, it initially decreases for a short distance. The reason is that a large ξ_i (or ξ_i') initially produces a large β value, which shortly settles down to an increasing trend. This nonsimilar behavior is in accord with the experimentally obtained β variation seen in Ref. 7.

E. Skin Friction and Heat Transfer

Reference 8 provides formulas for the skin friction and heat transfer at the wall, such as

$$\tau_w(s) = \left(\frac{\rho_e\mu_e u_e^3}{2\tilde{z}_i\bar{x}}\right)^{1/2} f''_w \tag{24a}$$

$$q_w(s) = \left(\frac{\rho_e\mu_e u_e}{2\tilde{z}_i\bar{x}}\right)^{1/2} (h_{oe} - h_{ow})G'_w \tag{24b}$$

where the nondimensional length $\bar{x}$ is defined by

$$\bar{x}(s) = \frac{\xi_i + \int_0^s (\rho\mu u)_e\,ds}{(\rho\mu u)_e} \tag{25}$$

With the aid of Eqs. (13), (16), (20a), and (23), this relation takes the following form for each wall:

$$\bar{x}(M) = \frac{M_i \csc\theta^*(\xi_i + KJ)}{KFX_i^{(\gamma+1)/2(\gamma-1)}}, \quad \text{wall } a \tag{26a}$$

$$\bar{x}(M) = \frac{M_i \csc\theta^*(\xi_i' + KJ)}{KFX_i^{(\gamma+1)/2(\gamma-1)}}, \quad \text{wall } b \tag{26b}$$

$$\bar{x}(M) = \frac{M_i \csc\theta^*}{KFX_i^{(\gamma+1)/2(\gamma-1)}}\left(\xi_i' + \xi'_{A'B'} + K\int_{M_{B'}}^{M} \frac{I\,dM}{MX^2}\right), \quad \text{wall } c \tag{26c}$$

The parameters f''_w and G'_w are determined from a solution of the laminar boundary-layer equations, once β and g_w are known. By using Eqs. (13) and the relations

$$g_w = T_w/T_{oe} = T_w/T_o \tag{27a}$$

$$h_{oe} - h_{ow} = [\gamma/(\gamma-1)]R_g T_{oe}(1 - g_w) \tag{27b}$$

Eqs. (24) become

$$\tau_w(M) = \frac{\gamma p_o f''_w [M^3/(Re_o\bar{x})]^{1/2}}{[2(\gamma-1)]^{1/4} X^{(5\gamma-3)/4(\gamma-1)}} \tag{28a}$$

$$q_w(M) = \frac{\gamma p_o(1-g_w)G'_w[(\gamma R_g T_o M)/(Re_o\bar{x})]^{1/2}}{[2(\gamma-1)^5]^{1/4} X^{(3\gamma-1)/4(\gamma-1)}} \tag{28b}$$

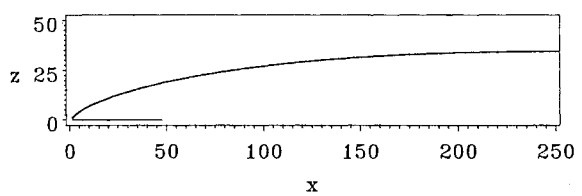

Fig. 3 Distribution of β along the nozzle walls when $M_i = 2$, $M_f = 6$, and $\gamma = 1.4$ for three $\xi_i\,(=\xi_i')$ values.

F. Boundary-Layer Thicknesses

From Ref. 8, the boundary-layer thicknesses are given by the following relations, with β, g_w, and S as parameters:

$$\Upsilon\delta = \eta_{ev} + \frac{1}{(1+\beta)(1-S)}\{S(f''_w + C_v) - (1-g_w)[1+\beta(1-S)]C_t\}$$

$$\Upsilon\delta_t = \eta_{et} + \frac{1}{(1+\beta)(1-S)}\{S(f''_w + C_v) - (1-g_w)[1+\beta(1-S)]C_t\}$$

$$\Upsilon\delta^* = \frac{1}{(1+\beta)(1-S)}\{Sf''_w + [1 + \beta(1-S)][C_v - (1-g_w)C_t]\}$$

$$\Upsilon\theta = \frac{1}{1+\beta}\{f''_w - \beta[C_v - (1-g_w)C_t]\}$$

$$\Upsilon\phi = G'_w$$

The parameters C_v, C_t, η_{ev}, η_{et}, f''_w, and G'_w are tabulated in the full-length version of Ref. 8, with β and g_w as entrees. However, we simply use the computer code of Ref. 8 as a subroutine, so that interpolation is not necessary. The dimensional nozzle inlet height $\tilde{z}_i$ is introduced in Υ, since $\bar{x}$ is nondimensional.

IV. Performance Parameters

Formulas are obtained for the thrust, lift, pitching moment, and heat transfer, per unit depth of flow. For an inviscid flow, the thrust, lift, and pitching moment are determined only by the pressure distribution along the walls. In this case, the momentum theorem can be used to obtain the thrust and lift.[4] However, for a viscous flow there is a change in the inviscid parameters, and the theorem does not easily yield these changes. Furthermore, it does not provide the distribution of quantities of interest along the walls, which is a central concern of this paper. An alternative approach is to use a direct integration along the walls of local values of the pressure, skin friction, and heat transfer. This approach has the advantages that viscous effects are easily incorporated, the wall distribution of heat transfer, etc., is obtained as a byproduct, and truncation of the upper or lower nozzle walls is readily performed.

A. Wall Section *a*

The force on wall a due to the pressure is given by

$$F_{pa} = -\int_0^s p\tilde{z}_i \, ds\hat{e}_z$$

which becomes, by using Eq. (15) and $p = p_o X^{-\gamma/(\gamma-1)}$,

$$F_{pa} = -p_o\tilde{z}_i \csc\theta^* \int_{M_i}^{M} \frac{\alpha(M^2-1)}{X^{(2\gamma-1)/(\gamma-1)}}\frac{dM}{M}\hat{e}_z \tag{29a}$$

The upper integral limit is a running variable in order to obtain a force distribution along the wall. The total force is found by replacing this limit with M_f. All integrals in this section are expressed in this manner.

The force due to the skin friction is

$$F_{\tau a} = \int_0^s \tau_w\tilde{z}_i \, ds\hat{e}_x$$

which becomes, by using Eqs. (15) and (28a),

$$F_{\tau a} = \frac{\gamma p_o\tilde{z}_i \csc\theta^*}{[2(\gamma-1)]^{1/4}Re_o^{1/2}} \int_{M_i}^{M} \frac{\alpha M^{1/2}(M^2-1)f''_w}{\bar{x}^{1/2}X^{(9\gamma-7)/4(\gamma-1)}} dM\hat{e}_x \tag{30a}$$

where $\bar{x}$ is provided by Eq. (26a), and $f''_w(M)$ is provided by a series of solutions along the wall of the boundary-layer equations. This integral is singular when $\bar{x} = 0$, which occurs when both $M = M_i$ and $\xi_i = 0$. Other subsequent integrals are singular in a similar situation. Reference 4 discusses how these singularities are resolved.

The pitching moment due to the pressure is

$$M_{pa} = \int_0^s (\tilde{z}_i x\hat{e}_x) \times (-p\tilde{z}_i \, ds\hat{e}_z)$$

which becomes, by using Eq. (15) and $p = p_o X^{-\gamma/(\gamma-1)}$,

$$M_{pa} = p_o\tilde{z}_i^2 \csc^2\theta^* \int_{M_i}^{M} \frac{\alpha^2(M^2-1)}{X^{(2\gamma-1)/(\gamma-1)}}\frac{dM}{M}\hat{e}_y \tag{31a}$$

The pitching moment about the origin of the x,y,z system, due to the skin friction, is

$$M_{\tau a} = 0 \tag{32a}$$

since the moment arm length is zero. As usual, a nose-lifting moment is taken as positive.

The wall heat transfer is

$$Q_a = \int_0^s q_w\tilde{z}_i \, ds$$

Substitution of Eqs. (15) and (28b) into this equation yields

$$Q_a = p_o\tilde{z}_i \csc\theta^* \left(\frac{\gamma^3 R_g T_o}{Re_o}\right)^{1/2} \frac{1-g_{wa}}{[2(\gamma-1)^5]^{1/4}} \times \int_{M_i}^{M} \frac{\alpha(M^2-1)G'_w \, dM}{\bar{x}^{1/2}M^{1/2}X^{(7\gamma-5)/[4(\gamma-1)]}} \tag{33a}$$

where g_{wa} is the value of g_w for wall a and is assumed to be a constant.

By normalizing Eqs. (29a)–(33a) with proper reference quantities that have the same dimensions as the performance parameters, we obtain

$$\hat{F}_{pa} = \frac{F_{pa}}{p_o\tilde{z}_i \csc\theta^*} = -H_1\hat{e}_z \tag{29b}$$

$$\hat{F}_{\tau a} = F_{\tau a}\Big/\left\{\frac{\gamma p_o\tilde{z}_i \csc\theta^*}{[2(\gamma-1)]^{1/4}Re_o^{1/2}}\right\} = H_2\hat{e}_x \tag{30b}$$

$$\hat{M}_{pa} = \frac{M_{pa}}{p_o\tilde{z}_i^2 \csc^2\theta^*} = H_3\hat{e}_y \tag{31b}$$

$$\hat{M}_{\tau a} = 0 \tag{32b}$$

$$\hat{Q}_a = Q_a\Big/\left\{\frac{\gamma p_o\tilde{z}_i \csc\theta^*(\gamma R_g T_o)^{1/2}(1-g_{wa})}{Re_o^{1/2}[2(\gamma-1)^5]^{1/4}}\right\} = H_4 \tag{33b}$$

The above H_i integrals are summarized in Table 1. These four H_i integrals are evaluated over the interval $M_i \le M \le M_f$.

B. Wall Section *b*

The forces, pitching moment, and heat transfer for this wall are obtained by the same procedure that is used for wall a. We thus have

$$\hat{F}_{pb} = \frac{F_{pb}}{p_o\tilde{z}_i \csc\theta^*} = H_1(-\sin\theta^*\hat{e}_x + \cos\theta^*\hat{e}_z) \tag{34}$$

$$\hat{F}_{\tau b} = F_{\tau b}\Big/\left\{\frac{\gamma p_o\tilde{z}_i \csc\theta^*}{[2(\gamma-1)]^{1/4}Re_o^{1/2}}\right\} = H_2(\cos\theta^*\hat{e}_x + \sin\theta^*\hat{e}_z) \tag{35}$$

$$\hat{M}_{pb} = \frac{M_{pb}}{p_o\tilde{z}_i^2 \csc^2\theta^*} = -H_3\hat{e}_y \tag{36}$$

Table 1 Summary of the H_i integrals

$$H_1 = \int_{M_i}^{M} \frac{\alpha(M^2-1)}{MX^{(2\gamma-1)/(\gamma-1)}}\,dM \qquad H_6 = \int_{M_{B'}}^{M} \frac{\alpha}{MX^{(2\gamma-1)/(\gamma-1)}} I\cos\theta\,dM$$

$$H_2 = \int_{M_i}^{M} \frac{\alpha M^{1/2}(M^2-1)f''_w}{\bar{x}^{1/2}X^{(9\gamma-7)/4(\gamma-1)}}\,dM \qquad H_7 = \int_{M_{B'}}^{M} \frac{\alpha M^{1/2}f''_w}{\bar{x}^{1/2}X^{(9\gamma-7)/4(\gamma-1)}} I\cos\theta\,dM$$

$$H_3 = \int_{M_i}^{M} \frac{\alpha^2(M^2-1)}{MX^{(2\gamma-1)/(\gamma-1)}}\,dM \qquad H_8 = \int_{M_{B'}}^{M} \frac{\alpha M^{1/2}f''_w}{\bar{x}^{1/2}X^{(9\gamma-7)/4(\gamma-1)}} I\sin\theta\,dM$$

$$H_4 = \int_{M_i}^{M} \frac{\alpha(M^2-1)G'_w}{\bar{x}^{1/2}M^{1/2}X^{(7\gamma-5)/4(\gamma-1)}}\,dM \qquad H_9 = \int_{M_{B'}}^{M} \frac{\alpha^2[1+\omega(M^2-1)^{1/2}]}{MX^{(2\gamma-1)/(\gamma-1)}} I\,dM$$

$$H_5 = \int_{M_{B'}}^{M} \frac{\alpha}{MX^{(2\gamma-1)/(\gamma-1)}} I\sin\theta\,dM \qquad H_{10} = \int_{M_{B'}}^{M} \frac{\alpha^2\omega M^{1/2}f''_w}{\bar{x}^{1/2}X^{(9\gamma-7)/4(\gamma-1)}} I\,dM$$

$$H_{11} = \int_{M_{B'}}^{M} \frac{\alpha G'_w}{\bar{x}^{1/2}M^{1/2}X^{(7\gamma-5)/4(\gamma-1)}} I\,dM$$

$$\hat{M}_{\tau b} = 0 \tag{37}$$

$$\hat{Q}_b = Q_b \Big/ \left\{\frac{\gamma p_o \tilde{z}_i \csc\theta^*(\gamma R_g T_o)^{1/2}(1-g_{wb})}{Re_0^{1/2}[2(\gamma-1)^5]^{1/4}}\right\} = H_4 \tag{38}$$

where $\theta^* = \theta^*_M, g_{wb}$ is assumed to be constant and may differ from the a or c values. The length $\bar{x}$ is given by Eq. (26b), and the range for the H_i integrals is $M_i \le M \le M_{B'}$.

C. Wall Section *c*

The force due to the pressure is given by

$$F_{pc} = \int_{S_{B'}}^{S} p\tilde{z}_i\,ds(-\sin\theta\hat{e}_x + \cos\theta\hat{e}_z)$$

where θ is the variable angle between this wall and the x axis. Substitution of Eq. (22) and $p = p_o X^{-\gamma/(\gamma-1)}$ yields

$$F_{pc} = p_o\tilde{z}_i\csc\theta^* \int_{M_{B'}}^{M} \frac{\alpha I\,dM}{MX^{(2\gamma-1)/(\gamma-1)}}(-\sin\theta\hat{e}_x + \cos\theta\hat{e}_z) \tag{39a}$$

The $\sin\theta$ and $\cos\theta$ terms are given by

$$\sin\theta = \frac{dz}{ds}, \qquad \cos\theta = \frac{dx}{ds}$$

where the differentials are provided by Eqs. (21) and (22). After simplification, these become

$$\sin\theta = \sin(\nu_f - \nu), \qquad \cos\theta = \cos(\nu_f - \nu)$$

in accord with a Prandtl-Meyer expansion. For brevity, we use θ instead of $\nu_f - \nu(M)$ in the following analysis and in Table 1.

The force due to the skin friction is given by

$$F_{\tau c} = \int_{S_{B'}}^{S} \tau_w\tilde{z}_i\,ds(\cos\theta\hat{e}_x + \sin\theta\hat{e}_z)$$

With the aid of Eqs. (22) and (28a), this becomes

$$F_{\tau c} = \frac{\gamma p_o\tilde{z}_i\csc\theta^*}{[2(\gamma-1)]^{1/4}Re_o^{1/2}} \int_{M_{B'}}^{M} \frac{\alpha M^{1/2}f''_w I\,dM}{\bar{x}^{1/2}X^{(9\gamma-7)/4(\gamma-1)}} \times(\cos\theta\hat{e}_x + \sin\theta\hat{e}_z) \tag{40a}$$

The pitching moment due to the pressure is

$$M_{pc} = \int_{S_{B'}}^{S} [\tilde{z}_i(x\hat{e}_x + z\hat{e}_z)] \times [p\tilde{z}_i\,ds(-\sin\theta\hat{e}_x + \cos\theta\hat{e}_z)]$$

From Eqs. (9), we have

$$x\cos\theta + z\sin\theta = \alpha\csc\theta^*[1+\omega(M^2-1)^{1/2}]$$

where $\nu_f - \nu$ is again replaced with θ. By using Eq. (22) and the above result, M_{pc} becomes

$$M_{pc} = -p_o\tilde{z}_i^2\csc^2\theta^* \int_{M_{B'}}^{M} \frac{\alpha^2[1+\omega(M^2-1)^{1/2}]}{MX^{(2\gamma-1)/(\gamma-1)}} I\,dM\hat{e}_y \tag{41a}$$

Similarly, the pitching moment produced by the skin friction is given by

$$M_{\tau c} = \int_{S_{B'}}^{S} [\tilde{z}_i(x\hat{e}_x + z\hat{e}_z)] \times [\tau_w\tilde{z}_i\,ds(\cos\theta\hat{e}_x + \sin\theta\hat{e}_z)]$$

Using Eqs. (9), we have

$$-x\sin\theta + z\cos\theta = \alpha\omega\csc\theta^*$$

Hence, $M_{\tau c}$ becomes, by using Eqs. (22) and (28a),

$$M_{\tau c} = \frac{\gamma p_o\tilde{z}_i^2\csc^2\theta^*}{[2(\gamma-1)]^{1/4}Re_o^{1/2}} \int_{M_{B'}}^{M} \frac{\alpha^2\omega M^{1/2}f''_w}{\bar{x}^{1/2}X^{(9\gamma-7)/4(\gamma-1)}} I\,dM\hat{e}_y \tag{42a}$$

The heat transfer at this wall is given by

$$Q_c = \int_{S_{B'}}^{S} q_w\tilde{z}_i\,ds$$

By substituting Eqs. (22) and (28b), we obtain

$$Q_c = \gamma p_o\tilde{z}_i\csc\theta^*\left(\frac{\gamma R_g T_o}{Re_o}\right)^{1/2}\frac{1-g_{wc}}{[2(\gamma-1)^5]^{1/4}} \times \int_{M_{B'}}^{M} \frac{\alpha G'_w I\,dM}{\bar{x}^{1/2}M^{1/2}X^{(7\gamma-5)/4(\gamma-1)}} \tag{43a}$$

The above equations are normalized and can be written as

$$\hat{F}_{pc} = \frac{F_{pc}}{p_o\tilde{z}_i\csc\theta^*} = -H_5\hat{e}_x + H_6\hat{e}_z \tag{39b}$$

$$\hat{F}_{\tau c} = F_{\tau c}\Big/\left\{\frac{\gamma p_o\tilde{z}_i\csc\theta^*}{[2(\gamma-1)]^{1/4}Re_o^{1/2}}\right\} = H_7\hat{e}_x + H_8\hat{e}_z \tag{40b}$$

$$\hat{M}_{pc} = \frac{M_{pc}}{p_o\tilde{z}_i^2\csc^2\theta^*} = -H_9\hat{e}_y \tag{41b}$$

$$\hat{M}_{\tau c} = M_{\tau c}\Big/\left\{\frac{\gamma p_o\tilde{z}_i^2\csc^2\theta^*}{[2(\gamma-1)]^{1/4}Re_o^{1/2}}\right\} = H_{10}\hat{e}_y \tag{42b}$$

$$\hat{Q}_c = Q_c \Big/ \left\{ \frac{\gamma p_o \tilde{z}_i \csc\theta^* (\gamma R_g T_o)^{1/2}(1-g_{wc})}{Re_o^{1/2}[2(\gamma-1)^5]^{1/4}} \right\} = H_{11} \quad (43b)$$

These H_i integrals are evaluated over the interval $M_{B'} \le M \le M_{tr}$, where the truncation Mach number M_{tr} satisfies $M_{B'} < M_{tr} \le M_f$. The upper limit of integration depends on the amount of truncation, which is determined by various design considerations.

D. Nondimensional Performance Parameters

We define the thrust coefficient as

$$C_F = \frac{\text{thrust when discharging into vacuum}}{p_o \tilde{R}_i \theta^*}$$

which is in accord with the usual sonic throat definition, and where the arc length $\tilde{R}_i\theta^*$ equals $\tilde{z}_i\theta^*\csc\theta^*$. The nondimensional thrust coefficient is obtained by summing up the force components in the x-direction for the three walls, with the result

$$C_F = \text{thrust}/(p_o \tilde{z}_i \theta^* \csc\theta^*) = \text{thrust}/F_r = C_{F\,\text{inv}} + C_{F\,\text{vis}}$$

$$C_{F\,\text{inv}} = (1/\theta^*)[\sin\theta^* H_1(M_{B'}) + H_5(M_{tr})]$$

$$C_{F\,\text{vis}} = -\gamma/\{[2(\gamma-1)]^{1/4} Re_o^{1/2}\theta^*\} \times [H_2(M_f) + \cos\theta^* H_2(M_{B'}) + H_7(M_{tr})]$$

Similarly, by summing up the force components in the z direction, the nondimensional lift coefficient is obtained:

$$C_L = \text{lift}/F_r = C_{L\,\text{inv}} + C_{L\,\text{vis}}$$

$$C_{L\,\text{inv}} = (1/\theta^*)[-H_1(M_f) + \cos\theta^* H_1(M_{B'}) + H_6(M_{tr})]$$

$$C_{L\,\text{vis}} = \gamma/\{[2(\gamma-1)]^{1/4} Re_o^{1/2}\theta^*\} \times [\sin\theta^* H_2(M_{B'}) + H_8(M_{tr})]$$

The nondimensional pitching moment coefficient is obtained as

$$C_M = \frac{\text{pitching moment}}{p_o \tilde{z}_i^2 \theta^* \csc^2\theta^*} = \frac{\text{pitching moment}}{M_r} = C_{M\,\text{inv}} + C_{M\,\text{vis}}$$

$$C_{M\,\text{inv}} = (1/\theta^*)[H_3(M_f) - H_3(M_{B'}) - H_9(M_{tr})]$$

$$C_{M\,\text{vis}} = \frac{\gamma H_{10}(M_{tr})}{[2(\gamma-1)]^{1/4} Re_o^{1/2}\theta^*}$$

The pitching moment is normalized by the force $p_o(\tilde{R}_i\theta^*)$, per unit depth, and the length $\tilde{R}_i$. Finally, we obtain the nondimensional total heat transfer as

$$C_Q = \frac{\text{total heat transfer}}{p_o \tilde{z}_i \theta^* \csc\theta^* (R_g T_o)^{1/2}} = \frac{\text{total heat transfer}}{Q_r}$$

$$= \frac{\gamma^{3/2}[(1-g_{wa})H_4(M_f) + (1-g_{wb})H_4(M_{B'}) + (1-g_{wc})H_{11}(M_{tr})]}{[2(\gamma-1)^5]^{1/4} Re_o^{1/2}\theta^*}$$

V. Results and Discussion

Three nominal cases are considered for which the input parameters are $\gamma = 1.4$, $R_g = 287$ kJ/kg-K, $C_\mu = 5.82 \times 10^{-8}$ kg/m-s-K, $\tilde{z}_i = 4$ cm, $p_o = 2$ atm, $T_o = 3000$ K, $T_{wa} = 450$ K, $T_{wb} = T_{wc} = 300$ K, and $M_{tr} = M_f$. The gas is air and C_μ is based on the Sutherland equation evaluated at 375 K. Since M_{tr} equals M_f, no truncation is involved. Other conditions are shown in Table 2, where the nominal cases are denoted by a b superscript. For convenience, we hereafter set $\xi_i = \xi_i'$; this choice is not necessary. For cases 101–103, ξ_i equals zero to avoid β becoming infinite in Eq. (19) when $M = 1$. For cases 201–203 and the subsequent cases, ξ_i is approximately 50, 100, and 250% of the change in ξ provided by wall a. For case 205, the key parameters are $g_{wa} = 0.15$, $g_{wb} = g_{wc} = 0.1$, $\theta_m^* = 41.6$ deg, $\dot{m} = 3.88$ kg/m-s, $K = 2.33 \times 10^{-2}$ kg^2/m^2-s^2, $M_{B'} = 2.69$, $Re_o = 1.32 \times 10^5$, $x_B - x_i = 46.3$, $x_f - x_i = 250$, and $z_f = 34.5$. We shall vary γ, g_{wa}, ξ_i $(=\xi_i')$, M_i, M_f, and M_{tr} about the nominal cases. The dependence on Re_o is obtained from the above equations.

Figures 4 and 5 show the inviscid thrust and lift coefficients vs M_f for the M_i values of the nominal cases. The leveling off occurs when the exit velocity approaches its maximum value. The sharp break in the C_L and C_F curves occurs when point B' separates from point A' and the slope of θ^*, with respect to M_f, changes discontinuously (see Fig. 2). Observe that C_L often exceeds C_F, sometimes by a substantial margin. Another important observation concerning these figures is the rapid

Table 2 Input conditions and the reference force, moment, and heat transfer for the cases considered

Case	M_i	M_f	p_o, atm	ξ_i (or ξ_i'), kg-N/m^3	F_r, N/m	M_r, N	Q_r, J/s-m
101	1	4	1	0	4.51 + 3[a]	2.53 + 2	4.19 + 6
102[b]	——	——	2	——	9.02 + 3	5.06 + 2	8.37 + 6
103	——	——	5	——	2.26 + 4	1.27 + 3	2.09 + 7
201	2	6	1	1.0 − 2	4.43 + 3	2.67 + 2	4.11 + 6
202	——	——	——	2.0 − 2	——	——	——
203	——	——	——	5.0 − 2	——	——	——
204	——	——	2	1.0 − 2	8.86 + 3	5.34 + 2	8.22 + 6
205[b]	——	——	——	2.0 − 2	——	——	——
206	——	——	——	5.0 − 2	——	——	——
207	——	——	5	1.0 − 2	2.22 + 4	1.34 + 3	2.06 + 7
208	——	——	——	2.0 − 2	——	——	——
209	——	——	——	5.0 − 2	——	——	——
301	4	8	1	1.0 − 3	4.24 + 3	3.41 + 2	3.94 + 6
302	——	——	——	2.0 − 3	——	——	——
303	——	——	——	5.0 − 3	——	——	——
304	——	——	2	1.0 − 3	8.48 + 3	6.82 + 2	7.87 + 6
305[b]	——	——	——	2.0 − 3	——	——	——
306	——	——	——	5.0 − 3	——	——	——
307	——	——	5	1.0 − 3	2.12 + 4	1.71 + 3	1.97 + 7
308	——	——	——	2.0 − 3	——	——	——
309	——	——	——	5.0 − 3	——	——	——

[a]Read as 4.51×10^3.

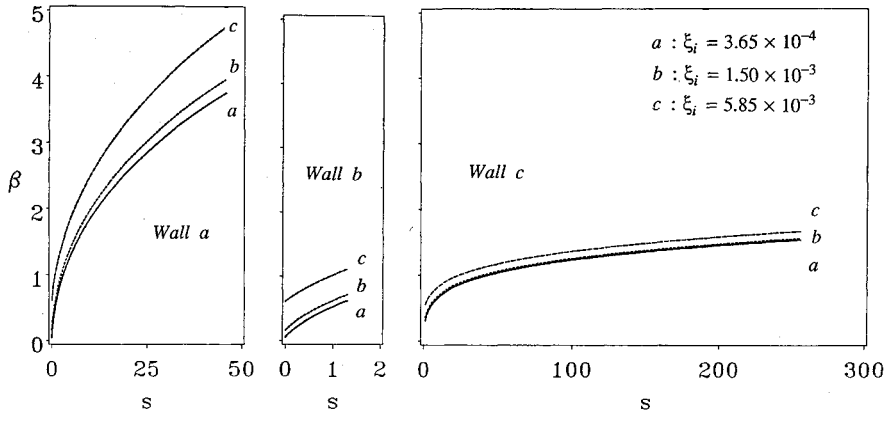

Fig. 4 Nondimensional inviscid thrust coefficient vs M_f with $\gamma = 1.4$.

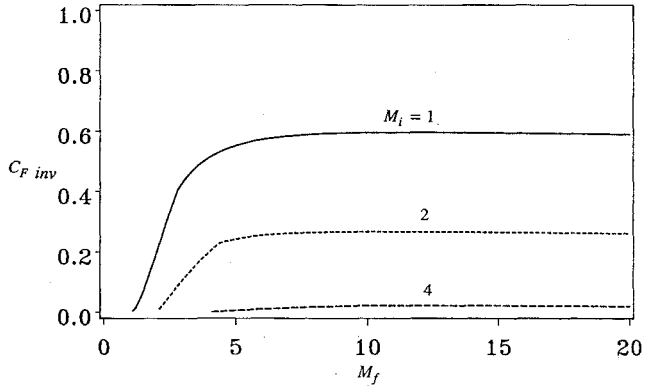

Fig. 5 Nondimensional inviscid lift coefficient vs M_f with $\gamma = 1.4$.

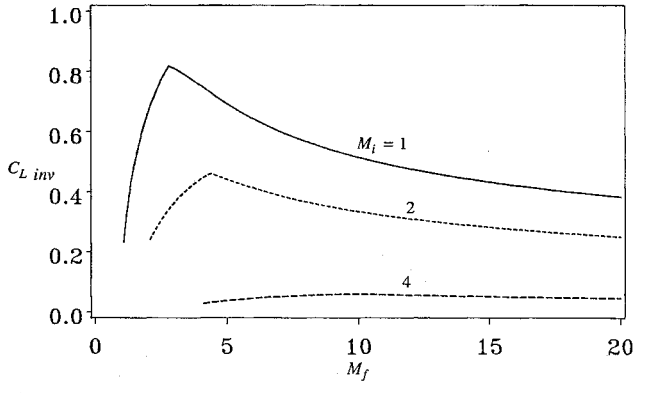

Fig. 6 Distribution of the thrust coefficient along the nozzle walls for case 205.

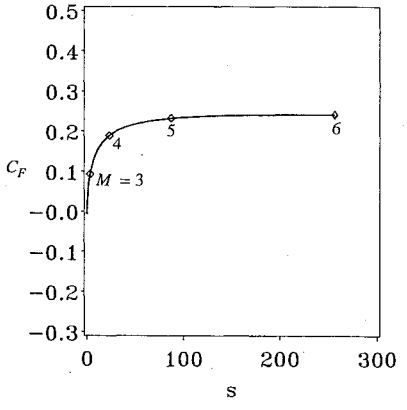

Fig. 7 Distribution of the lift coefficient along the nozzle walls for case 205.

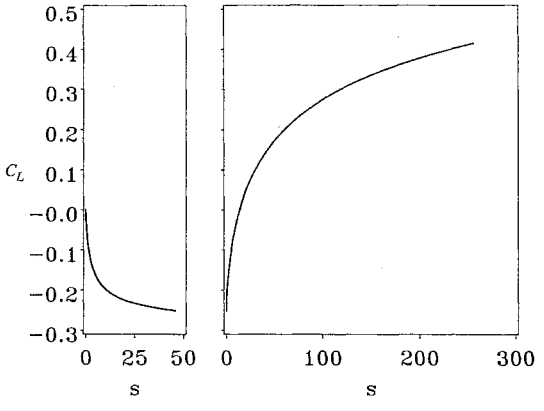

Fig. 8 Distribution of the pitching moment coefficient along the nozzle walls for case 205.

decrease in both coefficients with increasing M_i. This is primarily caused by the decrease in pressure, with a fixed p_o value, when M_i increases. As indicated in Ref. 9, an optimum nozzle inlet Mach number for thrust is unity.

Figures 6–8 show the distribution with nondimensional wall arc length of the performance parameters for case 205. The figures consist of two panels; the left one is for wall *a* and the right one is for walls *b* and *c*. The wall *a* panel is not provided when the parameter is zero or negligible; consequently, Fig. 6 shows the thrust only along walls *b* and *c*. The curve represents the accumulated thrust up to the point concerned, including the very slight initial negative thrust from wall *a*. This interpretation applies to all subsequent figures of this type. As seen in the figure, most of the thrust is obtained from the upstream part of the upper wall. Also shown are the Mach number values at several wall locations.

Figure 7 provides the distribution of lift along the nozzle walls, where wall *a* generates a negative lift. The value of lift at the beginning of the upper wall starts with the value at the end of wall *a*. Sufficient lift is generated by the upper wall to more than compensate for the negative lift of wall *a*. This result is in accord with Figs. 4 and 5, since viscous effects on the lift, thrust, and pitching moment are slight for case 205.

Figure 8 shows that walls *b* and *c* generate a negative pitching moment about the origin shown in Fig. 1. This moment is counter to the positive pitching moment of the forebody.

As expected, the ξ_i variation in Table 2 produces only small changes in C_F, C_L, and C_M.[4] However, changes in ξ_i cause a significant change in β (see Fig. 3), and in the heat transfer, as shown in Fig. 9. Most of the heat transfer occurs on the upstream part of walls *a* and *b*, and active cooling may be required. For example, when $\gamma = 1.4$ the maximum heat transfer rates, for case 205 at the start of walls *a* and *b*, are 286 kW/m^2 and 300 kW/m^2, respectively. On most of the upper nozzle wall, however, the rate of heat transfer is

moderate. The change in C_Q with ξ_i is not negligible; increasing ξ_i reduces the heat transfer.

The heat transfer, of course, depends on the assumed wall temperatures. For instance, case 205 has been run with T_{wa} increased from 450 K ($g_{wa} = 0.15$) to 750 K ($g_{wa} = 0.25$), leaving T_{wb} and T_{wc} at their nominal values. With this change, C_Q decreases from 1.06×10^{-2} to 9.61×10^{-3}, and the change in other performance parameters is even smaller. The percentage change in C_Q is not large because only wall a is affected.

The velocity boundary-layer thickness δ is shown in Fig. 10 for cases 204, 205, and 206. This thickness increases rapidly due to the increase of the speed parameter S. At the inlet of the nozzle, as seen in the inset, there is an appreciable spread for the three ξ_i cases. The relative difference, however, decreases with distance.

Table 3 summarizes global results for case 205, where separate viscous and inviscid values are provided. Clearly, C_F, C_L, and C_M are barely altered by the boundary layer.

Table 4 provides similar viscous global results for the nominal cases. The untruncated nozzles associated with these cases are all different as indicated by the θ^* and $x_f - x_i$ columns. As M_i increases, there is a rapid decrease in the magnitudes of C_F, C_L, and C_M, in accord with Figs. 4 and 5. Since the normalizing reference values F_r, M_r, and Q_r depend on θ^*, they are slightly different for each case (see Table 2). Because of the large Mach number values in case 305, there is a sizable decrease in thrust due to viscous drag.[4] More important in this case is the breakdown of the thin boundary-layer assumption, as ascertained by the nondimensional displacement thicknesses at points B and C'.[4]

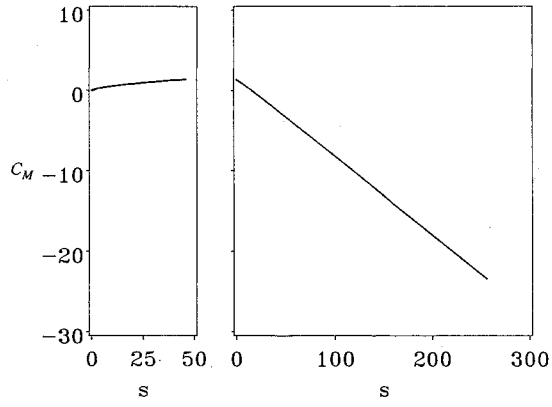

Fig. 9 Distribution of heat transfer coefficient along the nozzle walls for cases 204, 205, and 206.

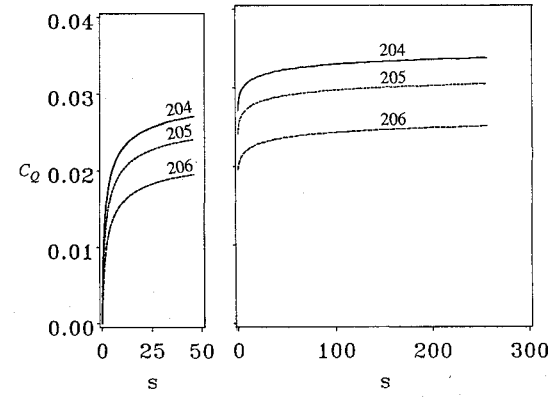

Fig. 10 Velocity boundary-layer thickness along the nozzle walls for cases 204, 205, and 206.

To reduce the size, weight, and drag of the vehicle, it is advisable to truncate the upper wall of the nozzle. The effect of such a truncation is shown in Table 5 for case 205. Note that when M_{tr} has decreased to 4.5 the upper wall terminates ahead of the lower wall. As expected from Fig. 6, the thrust decrease is quite modest for a sizable truncation. For instance, if $M_{tr} = 5$ and $\gamma = 1.4$ the thrust decreases by only 4.1%, whereas the upper wall length decreases by 67%! The small thrust decrease is attributable to the shallow angle of the downstream wall, where the pressure is sharply reduced, and to the skin friction along this wall. A still smaller value than 5 for M_{tr} might be attractive, except now both C_L and C_M start to rapidly decrease in magnitude. As expected from Fig. 9, there is little change in C_Q with truncation when $M_{tr} \geq 5$.

Table 5 repeats the computation with γ decreased to 1.3, which should be closer to an actual scramjet ratio of specific heats. While all other input conditions are the same as in case 205, the nozzle is significantly longer, as shown by $x_f - x_i$. This effect is also evident in Fig. 17.7 in Ref. 1; it takes a longer nozzle to expand a gas between prescribed Mach numbers when γ is closer to unity. With no truncation, the decrease in γ results in a moderate thrust increase, a negligible change in lift, and a large change in the pitching moment and heat transfer. With truncation, the relative changes are approximately the same, except for the lift, which decreases more rapidly at $\gamma = 1.3$ than at $\gamma = 1.4$.

At any M_{tr} value, C_Q in Table 5 is appreciably larger when $\gamma = 1.3$. This is partly due to the increase in surface area when $\gamma = 1.3$ as compared to $\gamma = 1.4$. The dominant effect ($\approx 40\%$), however, is due to the increased value for the specific heat at constant pressure. With a constant Prandtl number, this results in an equivalent increase in the thermal conductivity and, thus, in the heat transfer.

The last table (Table 6) shows the various boundary-layer thicknesses at points B and C' for the nominal cases, along with the nozzle exit height, z_f and wall a length. As evident at point C' for case 305, the thin boundary-layer assumption is invalid. Truncating wall c would reduce the boundary-layer thickness at its downstream edge. Nevertheless, the thin boundary-layer assumption is still invalid for this case by comparing the thicknesses with the height of the nozzle at point B.

Table 3 Performance parameters and heat transfer for case 205

Parameters	Wall a	Wall b	Wall c	Total
C_F	−4.13 − 3	5.71 − 2	1.90 − 1	2.43 − 1
$C_{F\,\mathrm{inv}}$	0	5.79 − 2	1.97 − 1	2.55 − 1
$C_{F\,\mathrm{vis}}$	−4.13 − 3	−8.50 − 4	−6.38 − 3	−1.14 − 1
C_L	−2.51 − 1	6.60 − 2	5.99 − 1	4.14 − 1
$C_{L\,\mathrm{inv}}$	−2.51 − 1	6.53 − 2	5.97 − 1	4.11 − 1
$C_{L\,\mathrm{vis}}$	0	7.60 − 4	2.12 − 3	2.88 − 3
C_M	1.38	−1.18 − 1	−2.47 + 1	−2.34 + 1
$C_{M\,\mathrm{inv}}$	1.38	−1.18 − 1	−2.47 + 1	−2.35 + 1
$C_{M\,\mathrm{vis}}$	0	0	3.81 − 2	3.81 − 2
C_Q	3.10 − 3	1.13 − 3	6.39 − 3	1.06 − 2

Table 4 Performance parameters and heat transfer for the three nominal cases

Case	C_F	C_L	C_M	C_Q	θ^*, deg	$x_f - x_i$
102	4.97 − 1	7.56 − 1	−1.44 + 1	2.39 − 2	4.55 + 1	5.98 + 1
205	2.43 − 1	4.14 − 1	−2.34 + 1	1.06 − 2	4.16 + 1	2.50 + 2
305	1.30 − 2	5.44 − 2	−1.54	3.95 − 3	2.98 + 1	1.81 + 2

Table 5 Effect of M_{tr} and γ on the performance parameters and heat transfer for case 205

γ	M_{tr}	$x_f - x_i$	C_F	C_L	C_M	C_Q
1.4	6.0	2.50 + 2	2.43 − 1	4.14 − 1	−2.34 + 1	1.06 − 2
	5.5	1.47 + 2	2.42 − 1	3.37 − 1	−1.34 + 1	9.96 − 3
	5.0	8.26 + 1	2.34 − 1	2.53 − 1	−6.97	9.21 − 3
	4.5	4.30 + 1	2.18 − 1	1.62 − 1	−3.00	8.36 − 3
	4.0	2.04 + 1	1.91 − 1	6.50 − 2	−7.05 − 1	7.38 − 3
	3.5	8.41	1.50 − 1	−3.49 − 2	5.13 − 1	6.27 − 3
1.3	6.0	5.39 + 2	2.87 − 1	4.15 − 1	−5.32 + 1	1.54 − 2
	5.5	2.81 + 2	2.84 − 1	3.13 − 1	−2.60 + 1	1.43 − 2
	5.0	1.37 + 2	2.71 − 1	2.05 − 1	−1.09 + 1	1.31 − 2
	4.5	6.10 + 1	2.45 − 1	9.20 − 2	−3.07	1.18 − 2
	4.0	2.42 + 1	2.05 − 1	2.06 − 2	6.33 − 1	1.03 − 2
	3.5	8.03	1.50 − 1	−1.26 − 1	2.19	8.64 − 3

Table 6 Nondimensional boundary-layer thicknesses at points B and C', nozzle length, and nozzle exit height when $\gamma = 1.4$

Point	Case	δ	δ_t	δ^*	θ^*	ϕ	z_f	$x_B - x_i$
B	102	2.67 − 1	2.98 − 1	6.60 − 2	3.50 − 2	5.32 − 2	——	1.40 + 1
	205	1.50	1.67	4.32 − 1	1.72 − 1	2.95 − 1	——	4.63 + 1
	305	2.31	2.49	1.15	1.91 − 1	3.17 − 1	——	3.39 + 1
C'	102	5.09 − 1	5.52 − 1	1.48 − 1	6.68 − 2	8.99 − 2	1.19 + 1	——
	205	3.65	3.93	1.59	3.69 − 1	5.30 − 1	3.45 + 1	——
	305	9.14	9.60	5.56	6.49 − 1	9.09 − 1	1.86 + 1	——

VI. Conclusions

Our principal findings are that the thrust and lift rapidly decrease as the nozzle's inlet Mach number increases above unity. The nozzle not only develops lift but this lift can exceed the thrust. The development of lift is proven by both the momentum theorem and by a straightforward integration of pressure along the wall surfaces. The nozzle also develops a substantial pitching moment that should partly counter the oppositely oriented moment developed by the forebody.

The heat transfer is most intense on the upstream edges of walls a and b. There is little loss in thrust when the upper wall is significantly truncated. Depending on the amount of truncation, the decrease in the lift and pitching moment is moderate. Finally, we observe that some of our results are sensitive to γ. In particular, decreasing γ from 1.4 to 1.3, with $M_{tr} = 5$, increases the magnitude of C_F, C_M, and C_Q, but decreases C_L. Because of its greater length, a low γ nozzle may have greater amount of truncation than a high γ nozzle.

Acknowledgment

The authors gratefully acknowledge the financial support of the NASA Langley Research Center under Grant NAG-1-886.

References

[1]Emanuel, G., *Gasdynamics: Theory and Applications*, AIAA Educational Series, New York, 1986.

[2]Argrow, B. M., and Emanuel, G., "Comparison of Minimum Length Nozzle," *Journal of Fluid Engineering*, Vol. 110, Sept. 1988, pp. 283–288.

[3]Argrow, B. M., "Computational Analysis of the Transonic Flow Field of Two-Dimensional Minimum Length Nozzles," Ph.D. Dissertation, Univ. of Oklahoma, Norman, OK, 1989.

[4]Bae, Y. Y., "Performance of An Aero-Space Plane Propulsion Nozzle," Ph.D. Dissertation, Univ. of Oklahoma, Norman, OK, 1989.

[5]Emanuel, G., "Supersonic Compressive Ramp Without Laminar Boundary-Layer Separation," *AIAA Journal*, Vol. 22, Jan. 1984, pp. 29–34.

[6]Smith, A. M. O., and Clutter, D. W., "Machine Calculation of Compressible Laminar Boundary Layers," *AIAA Journal*, Vol. 3, No. 9, 1965, pp. 639–647.

[7]Marvin, J. G., and Sinclair, A. R., "Convective Heating in Regions of Large Favorable Pressure Gradient," *AIAA Journal*, Vol. 5, Nov. 1967, pp. 1940–1948.

[8]Bae, Y. Y., and Emanuel, G., "Boundary-Layer Tables for Similar Compressible Flow," *AIAA Journal*, Vol. 27, Sept. 1989, pp. 1163–1164.

[9]Emanuel, G., "A First Scramjet Study," NASA CR-184965, 1989.